Hemisynthesis, crystal structure and inhibitory effect of sesquiterpenic thiosemicarbazones and thiazolidin-4-ones on the corrosion behaviour of stainless steel in 1 M H 2 SO 4 solution

Abdoullah Bimoussa, Yassine Koumya, Abdesselam Abouelfida, Moulay Youssef Ait Itto, Abdelaziz Benyaich, Olivier Mentré, El Mostafa Ketatni, Aziz Auhmani, Abdelwahed Auhmani

Hemisynthesis, crystal structure and inhibitory effect of sesquiterpenic thiosemicarbazones and thiazolidin-4-ones on the corrosion behaviour of stainless steel in 1 *M* H_2SO_4 solution

Abdoullah Bimoussa,[a] Yassine Koumya,[b] Abdesselam Abouelfida,[b] Moulay Youssef Ait Itto,[a] Abdelaziz Benyaich,[b] Olivier Mentre,[c] El Mostafa Ketatni,[d] Aziz Auhmani[a]* and Abdelwahed Auhmani[a]

[a]Laboratory of Organic Synthesis and Physico-Molecular Chemistry, Department of Chemistry, Faculty of Sciences Semlalia, PO Box 2390, Marrakech 40001, Morocco, [b]Laboratory of Physical Chemistry of Materials and Environment, Department of Chemistry, Faculty of Science Semlalia, Cadi Ayyad University, PO Box 2390, Marrakech, Morocco, [c]Univ. Lille, CNRS, Centrale Lille, ENSCL, Univ. Artois, UMR 8181 – UCCS – Catalysis and Solid Chemistry Unit, F-59000 Lille, France, and [d]Laboratory of Organic and Analytical Chemistry, University Sultan Moulay Slimane, Faculty of Science and Technology, PO Box 523, Beni-Mellal, Morocco. *Correspondence e-mail: a.auhmani@uca.ac.ma

Keywords: essential oil; sesquiterpene hydrocarbon; hemisynthesis; thiosemicarbazone; thiazolidinone; crystal structure; computational chemistry; C—H···Cl hydrogen bonding; corrosion; polarization; DFT; cyclic voltammetry.

CCDC reference: 1911992

Treatment of thiosemicarbazones prepared from sesquiterpenes with ethyl 2-bromoacetate in the presence of sodium acetate afforded the corresponding thiazolidin-4-ones. The structures of all the newly synthesized compounds were established by considering spectral and single-crystal X-ray diffraction data. The title compound, ethyl 2-((*Z*)-2-{(*Z*)-[(1a*R*,5a*R*,9a*S*)-1,1-dichloro-1a,5,5,7-tetramethyl-1a,2,3,4,5,5a,8,9-octahydro-1*H*-benzo[*a*]cyclopropa[*b*][7]annulen-8-ylidene]-hydrazono}-4-oxothiazolidin-3-yl)acetate, $C_{23}H_{31}Cl_2N_3O_3S$, **5**, crystallizes in the orthorhombic noncentrosymmetric space group $P2_12_12_1$ with $Z = 4$. Within the molecule in the crystal structure, the cyclohexene ring has an envelope conformation and the cycloheptane ring, to which it is fused, has a boat conformation. In the crystal, molecules are linked by C—H···Cl hydrogen bonds forming chains propagating along the *b*-axis direction. The absolute configuration of the molecule in the crystal could be fully confirmed from anomalous dispersion effects [Flack parameter = −0.04 (2)]. Thiosemicarbazones **1** and **2** are efficient inhibitors for steel corrosion in 1 *M* H_2SO_4 solution, with a maximum efficiency of 92.28% at 10^{-3} *M*. Furthermore, thiosemicarbazone compounds were found to be more efficient than thiazolidin-4-one derivatives. In addition, cyclic voltammetry was used to characterize the tested molecules, as well to estimate the experimental value of the energy band gap.

1. Introduction

Thiazolidinones are an important class of heterocycles because a considerable number of them manifest diverse pharmacological properties, such as antifungal (Srivastava *et al.*, 2005; Misra & Patnayak, 1971), antibacterial (Bondock *et al.*, 2006; Vicini *et al.*, 2006; Bondock *et al.*, 2007), antiviral (Rawal *et al.*, 2005), anticancer (Ottana *et al.*, 2005*a*,*b*; Gududuru *et al.*, 2004; Pyo *et al.*, 2001), anti-inflammatory (Vigorita *et al.*, 2003; Ottana *et al.*, 2002, 2005*a*,*b*), anthelmintic (Aries, 1974, 1975, 1976; Giraudon, 1972, 1973), antitubercular (Danila & Radu, 1978, 1979; Zubenky *et al.*, 1974, 1975), hypnotic (Chaudhary *et al.*, 1975, 1976), anticonvulsant (Parmar *et al.*, 1972; Shyam & Tiwari, 1977) and cardiovascular effects (Suzuki *et al.*, 1999; Nagar *et al.*, 1973). Furthermore, it is documented that organic compounds containing π electrons and heteroatoms, such as nitrogen, oxygen and sulfur, could be

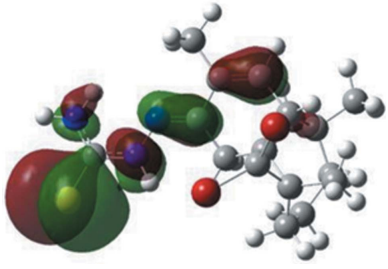

excellent as corrosion inhibitors (Gece, 2008; Idouhli *et al.*, 2018*a*,*b*; Singh & Chaudhary, 1996; Chaudhary *et al.*, 2007). Thus, recently, Idouhli *et al.* (2018*a*,*b*) reported that monoterpenic thiosemicarbazones are efficient inhibitors for steel corrosion in 1 *M* HCl. Mourya *et al.* (2013) also investigated a thiosemicarbazone derivative as a corrosion inhibitor of mild steel in 1 *N* HCl and 1 *N* H_2SO_4. The inhibitive action of some 1,3,4-thiadiazole derivatives against corrosion was investigated by Lebrini *et al.* (2007), Blajiev & Hubin (2004) and Bentiss *et al.* (2007). In continuation of our investigations of the hemisynthesis of new compounds with added value using sesquiterpene hydrocarbons extracted from the essential oil of *Cedrus atlantica*, we describe herein the hemisynthesis, the crystal structure and the effect of newly synthesized thiazolidin-4-one and thiosemicarbazone molecules on the corrosion behaviour of stainless steel. The quantum chemical calculations were also employed to link between the inhibition efficiency and the molecular properties of the tested compounds.

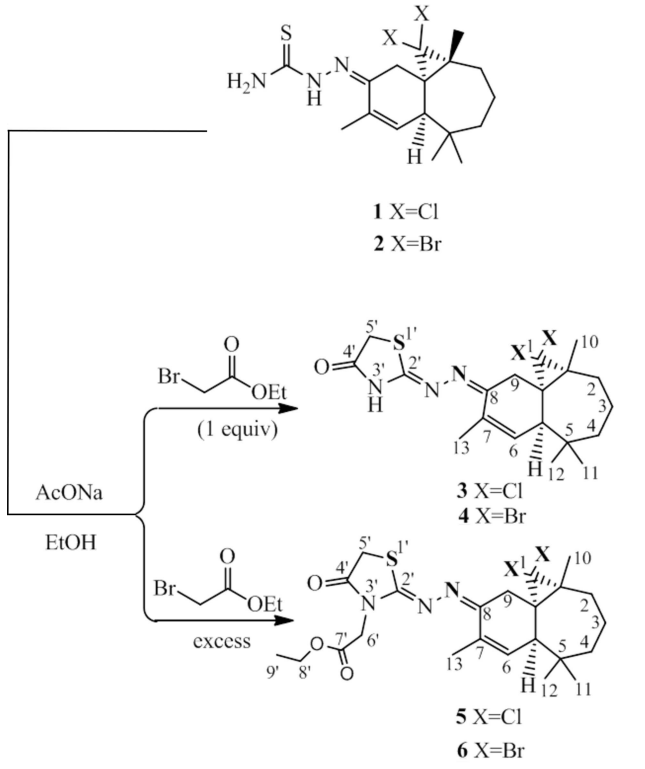

Scheme 1

2. Experimental

IR spectra were recorded on a Bruker Vertex 70 spectrophotometer using potassium bromide discs in the frequency range 4000–400 cm^{-1}. ^1H and ^{13}C NMR spectra were recorded on a Bruker Avance 300 (75) MHz spectrometer. Chemical shifts (δ, ppm) were reported with reference to $SiMe_4$ (^1H). Melting points were determined with a Kofler bench apparatus and are uncorrected. Elemental analyses were taken with an Elementar Vario EL-III Analyzer. All solvents were dried and distilled before use. Column chromatography was performed on silica gel 60 (70–230 mesh, Merck). Thin-layer chromatography (TLC) was carried out on Merck 0.2 mm silica gel 60 F254 analytical aluminium plates.

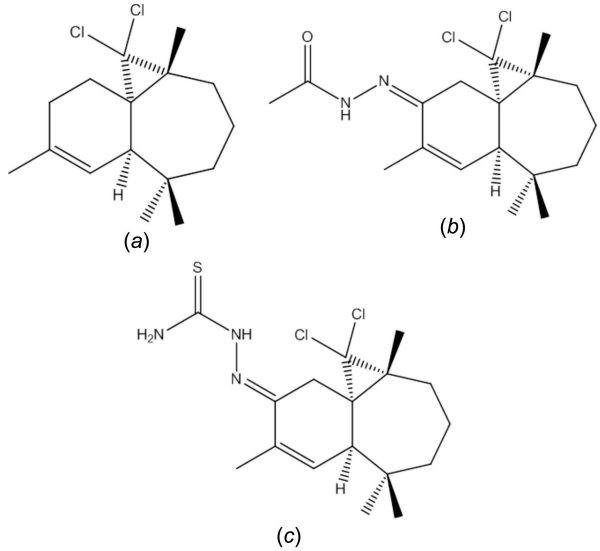

Scheme 2

2.1. Hemisynthesis

2.1.1. General procedure for the preparation of thiosemicarbazone 2. A mixture of enone (1 mmol) dissolved in ethanol (20 ml), thiosemicarbazide (2 mmol) and a few drops of H_2SO_4 were refluxed with magnetic stirring for 2 to 3 h. The yellow precipitate which formed was removed by filtration and recrystallized from EtOH solution to give the thiosemicarbazone (*Z*)-2-[(1a*R*,5a*R*,9a*S*)-1,1-dibromo-1a,5,5,7-tetramethyl-1a,2,3,4,5,5a,8,9-octahydro-1*H*-benzo[*a*]cyclopropa[*b*][7]annulen-8(9*H*)-ylidene]hydrazinecarbothioamide, **2**.

Analytical data for **2**: yield 65%; m.p. 183–184 °C; IR (KBr) ν_{max}/cm^{-1}: 3409 (NH_2), 3147 (NH), 2925 (C═C), 1592 (C═N), 1290 (C═S), 1066 (C—N); ^1H NMR (300 MHz, $CDCl_3$): δ 8.75, 7.28, 6.44 (3H, NH_2 and NH), 6.24 (1H, *d*, *J* = 7.22 Hz), 0.84 (3H, *s*), 1.01 (3H, *s*), 1.96 (3H, *s*), 1.82 (3H, *s*), 2.5 (1H, *d*, *J* = 7.9 Hz), 2.62 (2H, AB system, *J* = 18.2 Hz); ^{13}C NMR (75 MHz, $CDCl_3$): 60.44 (C-1), 33.74 (C-1a), 29.67 (C-2), 38.79 (C-3), 41.33 (C-4), 29.6 (C-5), 47.91 (C-5a), 135.84 (C-6), 133.22 (C-7), 147.37 (C-8), 21.35 (C-9), 38.79 (C-9a), 22.64 (C-10), 18.63 (C-11), 18.03 (C-12), 29.67 (C-13), 179.02 (C═S). Analysis calculated (%) for $C_{17}H_{25}Br_2N_3S$: C 44.07, H 5.44, N 9.07, S 6.92; found: C 44.04, H 5.37, N 9.03, S 6.89.

2.1.2. General method for the hemisynthesis of thiazolidin-4-ones 3, 4, 5 and 6. A mixture of thiosemicarbazone (1 mmol), ethyl 2-bromoacetate (1 mmol, 167 mg) in the cases of **3** and **4** (an excess of ethyl 2-bromoacetate in the cases of **5** and **6**), and anhydrous sodium acetate (4.5 mmol, 369 mg) in ethanol (30 ml) was stirred under reflux for 1 h until none of the starting materials was detected using TLC. The solvent was removed under reduced pressure. The residue was dissolved in water (100 ml) and extracted with ethyl acetate (3 × 50 ml). The organic layer was dried over Na_2SO_4 and concentrated *in vacuo*. The residue was purified by flash chromatography on silica gel using *n*-hexane–ethyl acetate (92:8 *v*/*v*) as eluent.

Analytical data for (*Z*)-2-{(*Z*)-[(1a*R*,5a*R*,9a*S*)-1,1-dichloro-1a,5,5,7-tetramethyl-1a,2,3,4,5,5a,8,9-octahydro-1*H*-benzo[*a*]-cyclopropa[*b*][7]annulen-8-ylidene]hydrazono}thiazolidin-4-one, **3.** Yield 52%; IR (KBr) ν_{max}/cm^{-1}: 3418 (NH), 2925 (C═C), 1724 (C═O), 1599 (C═N), 1554 (C═N), 1022 (C—N); ^{1}H NMR (300 MHz, $CDCl_3$): δ 0.86 (3H, *s*), 1.01 (3H, *s*), 1.20 (3H, *s*), 2.00 (3H, *s*), 2.46 (1H, *d*, *J* = 6.23 Hz), 2.7 (2H, AB system, *J* = 18.3 Hz), 6.23 (1H, *d*, *J* = 7.9 Hz), 3.75 (2H, *s*), 9.5 (NH, *s*); ^{13}C NMR (75 MHz, $CDCl_3$): δ 77.53 (C-1), 33.08 (C-1a), 29.90 (C-2), 29.70 (C-3), 38.77 (C-4), 46.05 (C-5a), 33.49 (C-5), 136.91 (C-6), 133.99 (C-7), 164.01 (C-8), 21.09 (C-9), 21.33 (C-9a), 14.16 (C-10), 17.95 (C-11), 16.05 (C-12), 29.70 (C-13), 161.09 (C-2′), 32.35 (C-5′), 173.67 (C-4′). Analysis calculated (%) for $C_{19}H_{25}Cl_2N_3OS$: C 55.07, H 6.08, N 10.14, S 7.74; found: C 54.99, H 6.03, N 10.04, S 7.69.

Analytical data for (*Z*)-2-{(*Z*)-[(1a*R*,5a*R*,9a*S*)-1,1-dibromo-1a,5,5,7-tetramethyl-1a,2,3,4,5,5a,8,9-octahydro-1*H*-benzo[*a*]-cyclopropa[*b*][7]annulen-8-ylidene]hydrazono}thiazolidin-4-one, **4.** Yield 62%; m.p. 194–195 °C; IR (KBr) ν_{max}/cm^{-1}: 3467 (NH), 2927 (C═C), 1721 (C═O), 1621 (C═N), 1458 (C═N), 1038 (C—N); ^{1}H NMR (300 MHz, $CDCl_3$): δ 0.8 (3H, *s*), 0.89 (3H, *s*), 1.29 (3H, *s*), 2.02 (3H, *s*), 2.61 (2H, AB system, *J* = 18.4 Hz), 6.23 (*d*, 1H, *J* = 8.10 Hz), 3.76 (2H, *s*), 8.9 (1H, *s*); ^{13}C NMR (75 MHz, $CDCl_3$): δ 58.57 (C-1), 33.26 (C-1a), 29.73 (C-2), 28.83 (C-3), 38.66 (C-4), 34.57 (C-5), 48.47 (C-5a), 136.32 (C-6), 134.30 (C-7), 163.43 (C-8), 21.41 (C-9), 38.66 (C-9a), 14.06 (C-10), 18.21 (C-11), 17.82 (C-12), 28.84 (C-13), 160.79 (C-2′), 33.03 (C-5′), 173.42 (C-4′). Analysis calculated (%) for $C_{19}H_{25}Br_2N_3OS$: C 45.34, H 5.01, N 8.35, S 6.37%; found: C 45.31, H 4.96, N 8.26, S 6.30.

Analytical data for ethyl 2-((*Z*)-2-{(*Z*)-[(1a*R*,5a*R*,9a*S*)-1,1-dichloro-1a,5,5,7-tetramethyl-1a,2,3,4,5,5a,8,9-octahydro-1*H*-benzo[*a*]cyclopropa[*b*][7]annulen-8-ylidene]hydrazono}-4-oxothiazolidin-3-yl)acetate, **5.** Yield 46%; m.p. 252–253 °C; IR (KBr) ν_{max}/cm^{-1}: 3446 (NH), 2924 (C═C), 1753 (C═O), 1728 (C—O), 1563 (C═N), 1624 (C═N), 1342 (C—O), 1017 (C—N); ^{1}H NMR (300MHz, $CDCl_3$): δ 0.78 (3H, *s*), 0.80 (3H, *s*), 1.20 (3H, *s*), 1.49 (3H, *t*, *J* = 7.03 Hz), 1.93 (3H, *s*), 2.68 (2H, AB system, *J* = 18.3 Hz), 3.75 (2H, *s*), 4.49 (2H, *q*, *J* = 7.03 Hz), 4.44 (2H, AB system, *J* = 16.6 Hz), 6.11 (1H, *d*, *J* = 7.9 Hz), 2.41 (1H, *d*, *J* = 7.9 Hz); ^{13}C NMR (75 MHz, $CDCl_3$): δ 78.36 (C-1), 30.18 (C-1a), 31.92 (C-2), 29.71 (C-3), 29.36 (C-4), 34.72 (C-5), 46.13 (C-5a), 136.61 (C-6), 134.13 (C-7), 162.18 (C-8), 21.37 (C-9), 22.37 (C-9a), 22.69 (C-10), 17.88 (C-11), 16.03 (C-12), 29.36 (C-13), 160.25 (C-2′), 173.85 (C-4′), 46.16 (C-5′), 43.96 (C-6′), 166.60 (C-7′), 61.67 (C-8′), 17.88 (C-9′). Analysis calculated (%) for $C_{23}H_{31}Cl_2N_3O_3S$: C 55.20, H 6.24, N 8.40, S 6.41; found: C 55.11, H 6.19, N 8.36, S 6.39.

Analytical data for ethyl 2-((*Z*)-2-{(*Z*)-[(1a*R*,5a*R*,9a*S*)-1,1-dibromo-1a,5,5,7-tetramethyl-1a,2,3,4,5,5a,8,9-octahydro-1*H*-benzo[*a*]cyclopropa[*b*][7]annulen-8-ylidene]hydrazono}-4-oxothiazolidin-3-yl)acetate, **6**. Yield 44%; IR (KBr) ν_{max}/cm^{-1}: 3447 (NH), 2931 (C═C), 1731 (C═O), 1608 (C—O), 1461 (C═N), 1623 (C═N), 1205 (C—O), 1030 (C—N); ^{1}H NMR (300 MHz, $CDCl_3$): δ 0.87 (3H, *s*), 1.01 (3H, *s*), 1.36 (3H, *s*), 1.55 (3H, *t*, *J* = 7.07 Hz), 2.02 (3H, *s*), 2.69 (2H, AB system, *J* = 18.4 Hz), 2.47 (1H, *d*, *J* = 8.18 Hz), 3.85 (2H, *s*), 4.21 (2H, *q*, *J* = 7.07 Hz), 4.51 (2H, AB system, *J* = 16.6 Hz), 6.22 (1H, *d*, *J* = 8.18 Hz); ^{13}C NMR (75 MHz, $CDCl_3$): δ 61.76 (C-1), 34.51 (C-1a), 32.50 (C-2), 28.72 (C-3), 38.65 (C-4), 33.24 (C-5), 43.94 (C-5a), 136.28 (C-6), 134.31 (C-7), 162.00 (C-8), 21.46 (C-9), 38.51 (C-9a), 21.10 (C-10), 18.18 (C-11), 17.19 (C-12), 29.79 (C-13), 160.29 (C-2′), 171.58 (C-4′), 48.48 (C-5′), 43.94 (C-6′), 166.63 (C-7′), 61.76 (C-8′), 17.91 (C-9′). Analysis calculated (%) for $C_{23}H_{31}Br_2N_3O_3S$: C 46.87, H 5.30, N 7.13, S 5.44; found: C 46.82, H 5.26, N 7.09, S 5.38.

Table 1
Experimental details.

Crystal data	
Chemical formula	$C_{23}H_{31}Cl_2N_3O_3S$
M_r	500.47
Crystal system, space group	Orthorhombic, $P2_12_12_1$
Temperature (K)	299
a, *b*, *c* (Å)	10.2769 (7), 12.2445 (7), 20.0804 (13)
V (Å^3)	2526.8 (3)
Z	4
Radiation type	Mo *K*α
μ (mm^{-1})	0.37
Crystal size (mm)	0.34 × 0.21 × 0.11
Data collection	
Diffractometer	Bruker DUO APEXII CCD
Absorption correction	Multi-scan (*SADABS*; Bruker, 2012)
T_{min}, T_{max}	0.710, 0.746
No. of measured, independent and observed [$I > 2\sigma(I)$] reflections	58280, 5789, 4306
R_{int}	0.056
(sin $\theta/\lambda)_{max}$ (Å^{-1})	0.650
Refinement	
$R[F^2 > 2\sigma(F^2)]$, $wR(F^2)$, *S*	0.038, 0.089, 1.03
No. of reflections	5789
No. of parameters	294
H-atom treatment	H-atom parameters constrained
$\Delta\rho_{max}$, $\Delta\rho_{min}$ (e Å^{-3})	0.26, −0.19
Absolute structure	Flack *x* determined using 1538 quotients $[(I^+) - (I^-)]/[(I^+) + (I^-)]$ (Parsons *et al.*, 2013)
Absolute structure parameter	−0.04 (2)

Computer programs: *DUO* in *APEX2* (Bruker, 2012), *SAINT* (Bruker, 2012), *SHELXS2014* (Sheldrick, 2008), *SHELXL2014* (Sheldrick, 2015), *ORTEP-3 for Windows* (Farrugia, 2012) and *DIAMOND* (Brandenburg & Putz, 2012).

2.2. Structure solution and refinement

The crystallographic data and experimental details for **5** are summarized in Table 1. H atoms were positioned geometrically and refined using a riding model, with C—H = 0.93–1.00 Å and U_{iso}(H) = 1.5U_{eq}(C) for methyl H atoms or 1.2U_{eq}(C) otherwise. The absolute structure was determined reliably based on the value of the Flack parameter [−0.04 (2)].

2.3. Electrochemical measurements and theoretical calculations

2.3.1. Material and methods. Potentiodynamic polarization measurements were carried out using voltalab potentiostat model PGZ301 with a three-electrode electrochemical cell and were recorded at a constant sweep rate of 1 mV s^{-1} in the potential range from −600 to 0 mV *versus* SCE. An electr

of 0.96 cm^2 exposed area was used as the working electrode (WE), together with a platinum counter-electrode (CE) and a saturated calomel electrode (SCE) as the reference electrode. The stainless steel specimens employed in the electrochemical cell have the following chemical composition: 69.10% Fe, 17.58% Cr, 9.01% Ni, 2.19% C, 0.54% Si and 0.39% Ti. Cyclic voltammetry experiments were carried out using a three-electrode cell consisting of a platinum working electrode, a platinum counter-electrode and a saturated calomel electrode as the reference electrode using a scan rate of 100 mV s^{-1}. The tested molecules were dissolved in 10^{-3} *M* acetonitrile. The supporting electrolyte was 0.2 *M* tetrabutylammonium perchlorate in anhydrous acetonitrile (CH_3CN).

2.3.2. Quantum chemical calculations. In order to determine the effect of the inhibitor structure on the corrosion process, density functional theory (DFT) was used to gain more insight into the molecular properties of the different tested derivatives. DFT quantum calculations have been carried out for the optimization of the molecules using the B3LYP function with a 6-31G(d) basis set (Becke, 1988; Lee *et al.*, 1988). The molecules were built with the *Gauss View* software (Version 09W; Frisch *et al.*, 2009). The detailed calculation method for the quantum chemical parameters has been described elsewhere (Klapper *et al.*, 2013).

3. Results and discussion

3.1. Synthesis

Several protocols for the preparation of thiazolidin-4-ones are used. Thus, a variety of these compounds was developed by using conventional one- and two-pot syntheses (Singh *et al.*, 1981; Cunico *et al.*, 2007). Another method for the synthesis of thiazolidin-4-ones is the use of a task-specific ionic liquid as the synthetic equivalent of an ionic liquid phase matrix (Fraga-Dubreuil & Bazureau, 2003). Holmes reported solution and polymer-supported methods to prepare thiazolidin-4-ones (Holmes *et al.*, 1995). This synthesis was performed by a one-pot three-component condensation under microwave irradiation (Dandia *et al.*, 2006; Desai & Mistry, 2006). Finally, an encoded thiazolidin-4-one library on a solid phase was reported by Maclean *et al.* (2004). In our approach to the synthesis of novel thiazolidin-4-ones, we tried to devise a process that could use a natural product thiosemicarbazone to react with ethyl 2-bromoacetate, as shown in Scheme 1.

Thus, treatment of thiosemicarbazone **1** (Auhmani *et al.*, 1999, 2002; Ourhriss *et al.*, 2005) or thiosemicarbazone **2** with an equivalent of ethyl 2-bromoacetate in the presence of sodium acetate afforded the nonsubstituted thiazolidinones (*Z*)-2-{(*Z*)-[(1a*R*,5a*R*,9a*S*)-1,1-dichloro-1a,5,5,7-tetramethyl-1a,2,3,4,5,5a,8,9-octahydro-1*H*-benzo[*a*]cyclopropa[*b*][7]annulen-8-ylidene]hydrazono}thiazolidin-4-one, **3**, and (*Z*)-2-{(*Z*)-[(1a*R*,5a*R*,9a*S*)-1,1-dibromo-1a,5,5,7-tetramethyl-1a,2,3,4,5,5a,-8,9-octahydro-1*H*-benzo[*a*]cyclopropa[*b*][7]annulen-8-ylidene]-hydrazono}thiazolidin-4-one, **4**. They were purified by flash chromatography with hexane as eluent and isolated as yellow liquids. The ^{1}H NMR spectrum of **3** showed a characteristic broad peak at 9.5 ppm assignable to the NH proton, followed by a doublet (*J* = 7.9 Hz) at 6.23 ppm for the H-6 proton and an additional singlet at 3.74 ppm for H-5′. The methylene protons on position 9 are magnetically non-equivalent and therefore display an AB system (*J* = 18.3 Hz) centred at 2.7 ppm. However, under similar conditions, but with an excess of ethyl 2-bromoacetate, thiosemicarbazones **1** and **2** provide ethyl 2-((*Z*)-2-{(*Z*)-[(1a*R*,5a*R*,9a*S*)-1,1-dichloro-1a,5,5,7-tetramethyl-1a,2,3,4,5,5a,8,9-octahydro-1*H*-benzo[*a*]cyclopropa-[*b*][7]annulen-8-ylidene]hydrazono}-4-oxothiazolidin-3-yl)acetate, **5**, and ethyl 2-((*Z*)-2-{(*Z*)-[(1a*R*,5a*R*,9a*S*)-1,1-dibromo-1a,5,5,7-tetramethyl-1a,2,3,4,5,5a,8,9-octahydro-1*H*-benzo[*a*]-cyclopropa[*b*][7]annulen-8-ylidene]hydrazono}-4-oxothiazolidin-3yl)acetate, **6**, in good yields. The structures of substituted thiazolidin-4-ones **5** and **6** were further characterized by FT–IR and ^{1}H and ^{13}C NMR spectroscopies. In the ^{1}H NMR spectrum of **5**, we note the absence of the characteristic signal of NH and the appearance of the signals of the acetate group. Thus, the corresponding methylene and methyl protons of the ethoxy group exhibit, respectively, a quadruplet (*J* = 7.03 Hz) at 4.49 ppm and a triplet (*J* = 7.03 Hz) at 1.49 ppm. The methylene proton at the 6′-position appears as an AB system (*J* = 16.6 Hz) at 4.44 ppm. The structure of **5** was confirmed by single-crystal X-ray diffraction analysis.

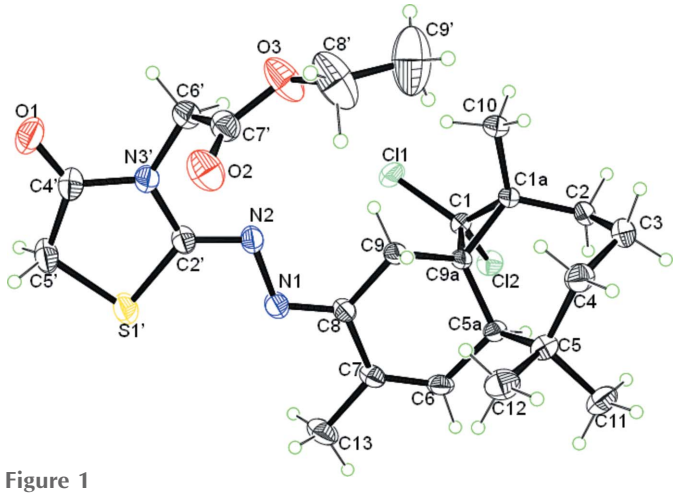

Figure 1
The molecular structure of the title molecule, **5**, showing the atom-labelling scheme and 30% probability displacement ellipsoids.

3.2. Crystal structure of the thiazolidin-4-one derivative

The compound is built from two fused six- and seven-membered rings which bear a dichlorocyclopropane group. An additional thiazolidinone hydrazone is linked to ethoxy–oxo-ethylidene units (Fig. 1). In the molecule, there are three chiral C atoms: C1a and C5a exhibits an *R* configuration and C9a exhibits an *S* configuration. The dihedral angle between the mean planes through the six- and seven-membered rings is 59.8 (2)°. The three-membered ring (C1/C1a/C9a) is nearly perpendicular to the mean plane of the six-membered ring (C5a/C6–C9/C9a), making a dihedral angle of 87.5 (2)°.

The six-membered cyclohexylidene ring has an approximate envelope conformation, with the puckering parameters *Q* =

Table 2
Selected geometric parameters (Å, °) for **5** (reported here) and **a–c** (reported previously).

Bond lengths	**5**	**a***	**b****	**c*****
Cl1—C1	1.768 (3)	1.757 (3)	1.763 (6)	1.769 (2)
Cl2—C1	1.768 (3)	1.762 (3)	1.766 (6)	1.761 (2)
N1—C8	1.287 (4)	–	1.283 (7)	1.288 (2)
C6—C7	1.331 (5)	1.318 (4)	1.342 (8)	1.326 (3)
C7—C8	1.472 (4)	1.486 (4)	1.474 (8)	1.472 (2)
C8—C9	1.509 (4)	1.511 (4)	1.512 (7)	1.504 (2)
Cl1—C1—Cl2	108.1 (2)	107.6 (2)	108.2 (3)	108.8 (1)
C7—C8—C9	118.6 (3)	114.8 (2)	118.2 (4)	119.6 (2)
C6—C7—C8	119.9 (3)	121.4 (3)	120.2 (4)	119.0 (2)
N1—C8—C7	117.0 (3)	–	116.3 (4)	116.3 (2)
N1—C8—C9	124.3 (3)	–	125.4 (5)	124.2 (2)

References: (*) Auhmani *et al.* (1999); (**) Benharref *et al.* (2016); (***) Ourhriss *et al.* (2005).

0.457 (3) Å, spherical polar angle θ = 55.6 (5)° and φ = 292.1 (5)°, whereas the seven-membered ring displays a boat conformation, with a total puckering amplitude $Q2$ = 1.139 (4) and $Q3$ = 0.035 (4) (Cremer & Pople, 1975).

Another point of interest is the comparison of the molecular structure of **5** with that of parent compound **a** (Auhmani *et al.*, 1999) and also with **b** (Benharref *et al.*, 2016) and **c** (Ourhriss *et al.*, 2005) (see Scheme 2). The C—Cl bond lengths [average 1.767 (3) Å] are in good agreement with the Cl—C bond length of 1.764 (6) Å reported for the related compounds (Table 2 and Scheme 2). The main difference between the conformations of these molecules is observed for the cyclohexene ring (between envelope and half-chair for **a**, half-chair for **b** and screw-boat for **c**).

As expected, the thiazolidine ring and all the atoms attached to it (plane A = S1′/C2′/N3′/C4′/C5′/N2/N1/O1/C6′) are roughly coplanar, with an r.m.s. deviation of 0.05 Å. Its mean plane makes a dihedral angle of 57.1 (1)° with the mean plane of the three-fused-ring system (C1/C1a/C2/C3/C4/C5/C5a/C6/C7/C8/C9/C9a).

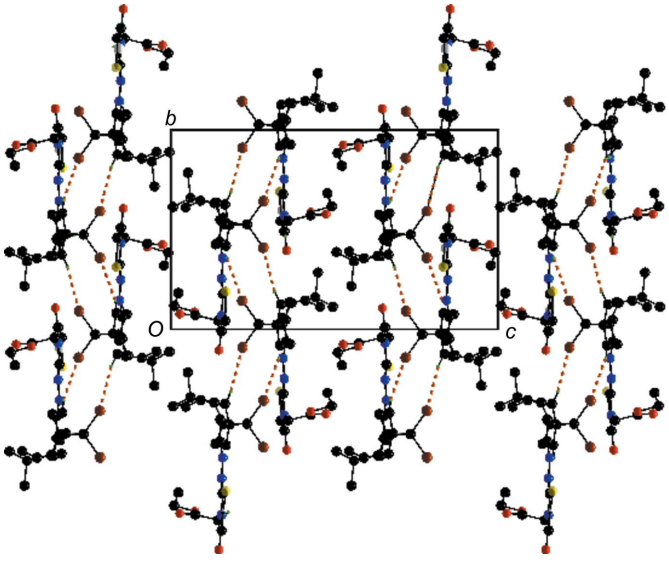

Figure 2
Packing and hydrogen-bonding interactions of the title compound viewed along the *b* axis. For clarity, only the H atoms involved in the hydrogen bonds (dashed lines) have been included.

Table 3
Comparison of main bond lengths (Å) and C═N—N═C torsions angles (°) in the title compound and related structures.

N1—N2	C2′—N2	N1—C8	S1′—C2′	N3′—C2′	C═N—N═C	Reference
1.413 (4)	1.275 (5)	1.288 (4)	1.744 (4)	1.383 (4)	−174.7 (3)	*a*
1.417 (3)	1.269 (3)	1.291 (3)	1.756 (3)	1.380 (3)	173.8 (3)	*b*
1.406 (2)	1.277 (2)	1.287 (2)	1.769 (2)	1.386 (2)	179.0 (2)	*c*
1.405 (3)	1.274 (3)	1.286 (4)	1.756 (3)	1.398 (3)	−168.9 (2)	*d*
1.407 (2)	1.281 (2)	1.291 (2)	1.761 (2)	1.392 (2)	179.4 (2)	*e*
1.414 (2)	1.278 (2)	1.278 (2)	1.749 (2)	1.367 (2)	−177.3 (2)	*f*
1.417 (7)	1.256 (7)	1.268 (8)	1.759 (5)	1.412 (8)	−177.6 (8)	*g*
1.410 (6)	1.279 (7)	1.279 (7)	1.767 (5)	1.364 (7)	174.9 (7)	*h*

References: (*a*) this study; (*b*) Gautam & Chaudhary (2015); (*c*) Hassan *et al.* (2017); (*d*) N'ait Ousidi *et al.* (2017); (*e*) Mague *et al.* (2014); (*f*) Ramachandran *et al.* (2009); (*g*) Gupta & Chaudhary (2013); (*h*) Gautam *et al.* (2013).

A comparison of the main C—N, N—N and C—S distances in the title compound and the structures formed by thiazolidine ring substituted by a hydrazone linked to a cyclohexyl ring as the main skeleton (Table 3) shows a good correlation: within the C═N—N═C fragment, the double bonds are located on C═N and the N—N distance is that of a single bond corresponding to a hydrazono group. The C═N—N═C torsion angles (Table 3) indicate that, in each case, the four atoms are nearly planar.

In the crystal, molecules are linked *via* C—H···Cl hydrogen bonds, forming chains propagating along the *b*-axis direction (Table 4 and Fig. 2).

3.3. Electrochemical and theoretical studies

3.3.1. Potentiodynamic polarization. Fig. 3 shows the potentiodynamic polarization curves of stainless steel (SS) in sulfuric acid in the absence and presence of the different synthesized molecules. The derived electrochemical parameters, such as the corrosion potential E_{corr}, the corrosion current density i_{corr} and the inhibition efficiency η (%), are listed in Table 5. The inhibition efficiency values were calculated by:

$$\eta\ (\%) = [(i_{corr} - i'_{corr}/i_{corr})] \times 100,$$

where i_{corr} and i'_{corr} are corrosion density without and with inhibitor, respectively.

It is clearly observed that thiosemicarbazones **1** and **2** both have reduced the corrosion current density and the corrosion potential was found to tend to more positive values with the addition of the inhibitor. The shift in the corrosion potential

Table 4
Hydrogen-bond geometry (Å, °).

D—H···*A*	*D*—H	H···*A*	*D*···*A*	*D*—H···*A*
C10—H10*A*···Cl2^{i}	0.96	2.79	3.557 (3)	137
C2—H2*B*···Cl1^{ii}	0.97	2.81	3.661 (3)	147

Symmetry codes: (i) $-x+2, y-\frac{1}{2}, -z+\frac{1}{2}$; (ii) $-x+2, y+\frac{1}{2}, -z+\frac{1}{2}$.

Table 5
Tafel parameters and corresponding inhibition efficiency derived from potentiodynamic polarization curves.

Inhibitor	E_{corr} (mV *versus* SCE)	i_{corr} (mA cm^{-2})	η (%)
Blank	−378.7	305.9	–
1	−330.3	112.8	63.12
3	−327.7	129.9	57.53
5	−369.4	202.5	33.80
2	−376.2	23.6	92.28
4	−327.8	187.4	38.73
6	−311.3	132.2	56.78

for both compounds is less than 85 mV with respect to the blank (Li *et al.*, 2012). Thus, both thiosemicarbazones act as mixed-type inhibitors. It should also be mentioned that both the anodic dissolution reaction and cathodic hydrogen evolution have been affected by the addition of the thiosemicarbazone. This trend may be explained by the fact that the addition of the inhibitor may block simultaneously the cathodic and anodic active sites (Patel *et al.*, 2013). The same behaviour has been observed with the thiazolidin-4-one derivatives; all these derivatives acted as mixed-type inhibitors. It can also be seen from Table 5 that thiazolidin-4-one derivatives do not show a good performance with respect to the thiosemicarbazone derivatives. In the case of the thiosemicarbazones, the maximum inhibition efficiency reached is 92% and was attained with the addition of 10^{-3} *M* of compound **2**. However, the maximum inhibition efficiency for the thiazolidin-4-one derivatives does not exceed 57%. The order of the inhibition efficiency η (%) was found to be: **2** > **1** > **3** > **6** > **4** > **5** (Table 5). These results reveal that thiosemicarbazone derivatives act as good corrosion inhibitors for SS corrosion in sulfuric acid; also, the inhibition efficiency depends greatly on the molecular structure of these derivatives.

3.3.2. Cyclic voltammetry measurements. For insights into the electrochemical activity of the tested molecules, as well as experimental calculations of the energy levels, the cyclic voltammetry measurements were performed in the wide potential range of −2000 to 2000 mV *versus* SCE. Fig. 4 shows that the cyclic voltammograms of the thiosemicarbazone molecules are different than those of the thiazolidin-4-one derivatives and display three anodic peaks and two cathodic peaks. However, the depicted electrochemical behaviour of the thiazolidin-4-one compounds is different due to the blocked electrochemical reactivity owing to the addition of new substituents to the molecular structure. All the cyclic voltammograms show an irreversible electrochemical process

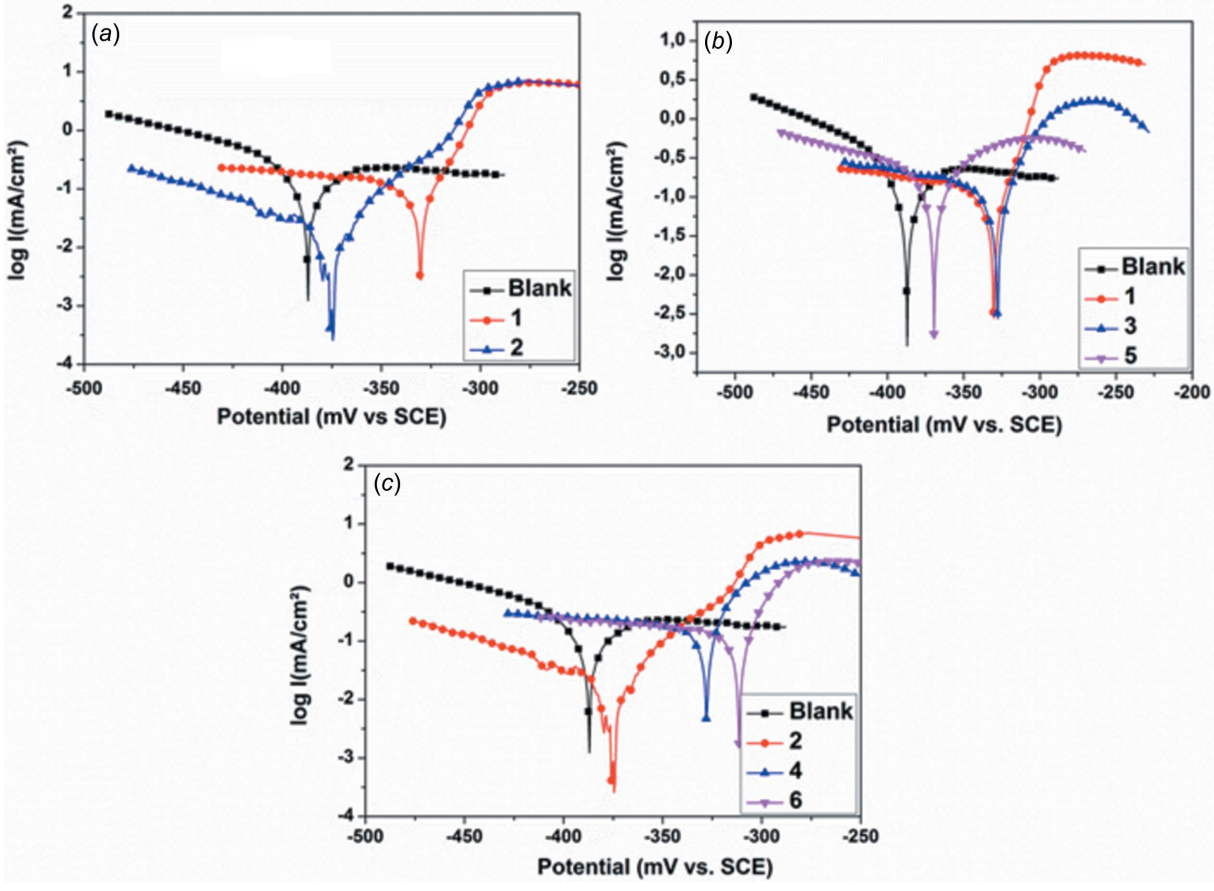

Figure 3
Potentiodynamic polarization curves of SS in sulfuric acid in the absence and presence of 10^{-3} *M* of different synthesized molecules, for (*a*) thiosemicarbazone derivatives, (*b*) thiazolidin-4-one derivatives having chloride functional groups and (*c*) thiazolidin-4-one derivatives having bromide functional groups.

Table 6
Cyclic voltammetry parameters for the different tested molecules in a solution of 0.2 *M* Et_4NClO_4/acetonitrile at 100 mV s^{-1}.

Molecule	E_{ox}^{onset}	E_{HOMO}	E_{red}^{onset}	E_{LUMO}	ΔE
1	0.235	−5.035	0.102	−4.902	0.133
2	−0.235	−4.565	−0.324	−4.476	0.089
3	0.537	−5.337	0.235	−5.035	0.302
4	0.271	−5.071	0.129	−4.929	0.142
5	0.572	−5.372	0.226	−5.026	0.346
6	0.182	−4.982	0.031	−4.831	0.151

because of the large separation between the anodic and cathodic peaks. The HOMO and LUMO energy levels of the different studied molecules were calculated from the onset oxidation potential (E_{ox}^{onset}) and the onset reduction potential (E_{red}^{onset}) using the following equations (Das *et al.*, 2015; Li *et al.*, 2011).

$$E_{HOMO} = -E_{ox}^{onset} - 4.8 \quad (1)$$
$$E_{LUMO} = -E_{red}^{onset} - 4.8 \quad (2)$$

The redox potentials, HOMO energy, LUMO energy and band gap for the different molecules are summarized in Table 6. The obtained results indicate that thiosemicarbazones **1** and **2** have the lowest band gap, which is in good agreement with the band gap deduced from the theoretical approach.

Table 7
Molecular properties of the thiosemicarbazone and thiazolidin-4-one derivatives calculated using DFT at the B3LYP/6-31G(d) basis set.

Molecule	**1**	**2**	**4**	**6**	**3**	**5**
E_{HOMO}	−0.201	−0.203	−0.216	−0.212	−0.217	−0.213
E_{LUMO}	−0.051	−0.053	−0.054	−0.053	−0.055	−0.053
ΔE	0.150	0.150	0.162	0.158	0.161	0.159
η	0.075	0.075	0.081	0.079	0.080	0.079
ΔE_T	−0.01875	−0.018	−0.020	−0.0198	−0.0202	−0.0198
ΔN	45.821	45.651	42.307	43.294	42.393	43.150
Dipole moment	7.295	6.696	3.738	3.834	3.881	4.085

Also, the experimental gap energy is roughly in the same order of magnitude when compared to the theoretical value.

3.3.3. Quantum chemical calculations. Generally, molecules having lower absolute values of the energy band gap ($\Delta E = |E_{LUMO} - E_{HOMO}|$) exhibit higher inhibition efficiencies since the energy to remove an electron from the last occupied orbital will be lower (Lebrini *et al.*, 2007). Table 7 summarizes the molecular properties of the molecules calculated using DFT at the B3LYP/6-31G(d) basis set. It is clear that the value of ΔE for the different studied molecules increases in the order **1** < **2** < **6** < **5** < **3** < **4**; this indicates that compounds **1** and **2** exhibit higher inhibition efficiencies. The dipole moment is another parameter of the electronic distribution in a molecule

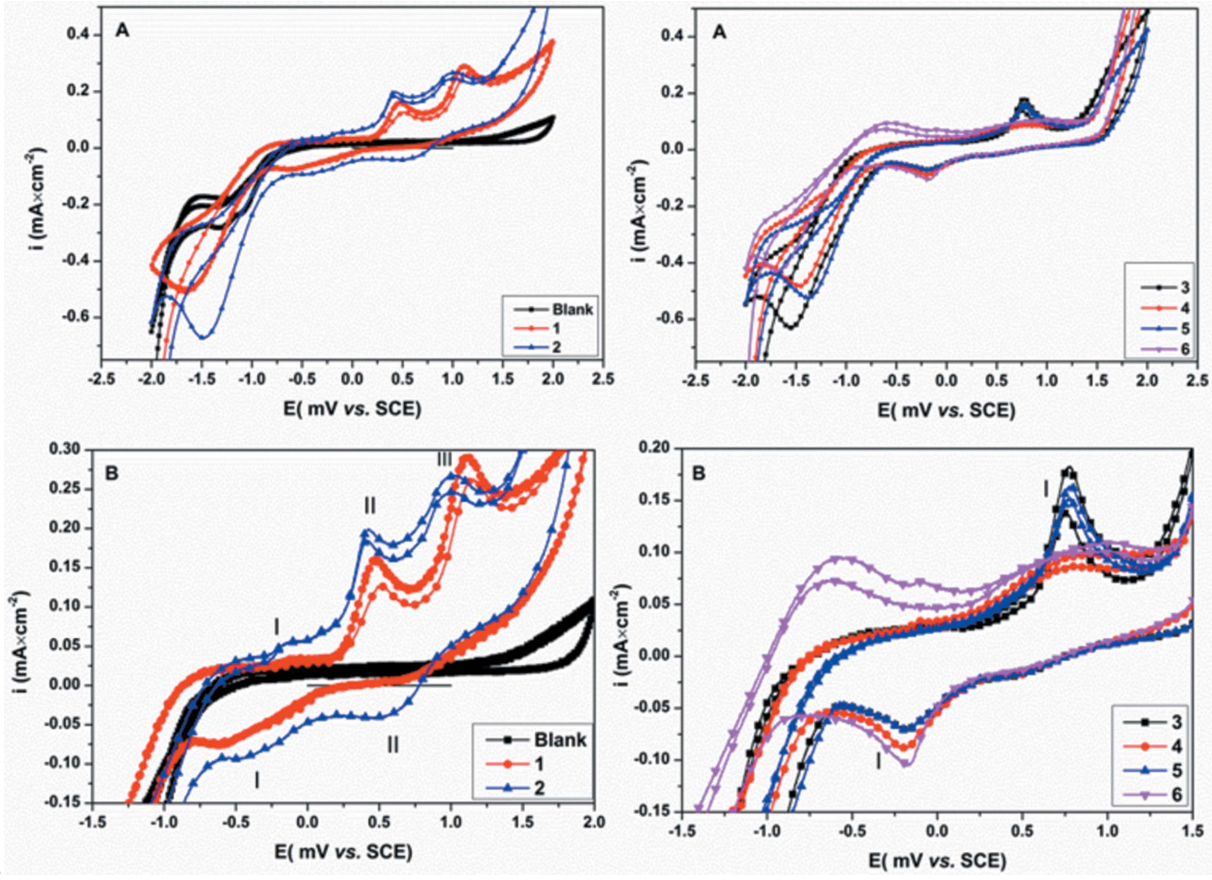

Figure 4
Cyclic voltammograms of (*a*) 10^{-3} *M* thiosemicarbazone compounds and (*b*) 10^{-3} *M* thiazolidin-4-one derivatives in a solution of 0.2 *M* Et_4NClO_4/acetonitrile at 100 mV s^{-1}.

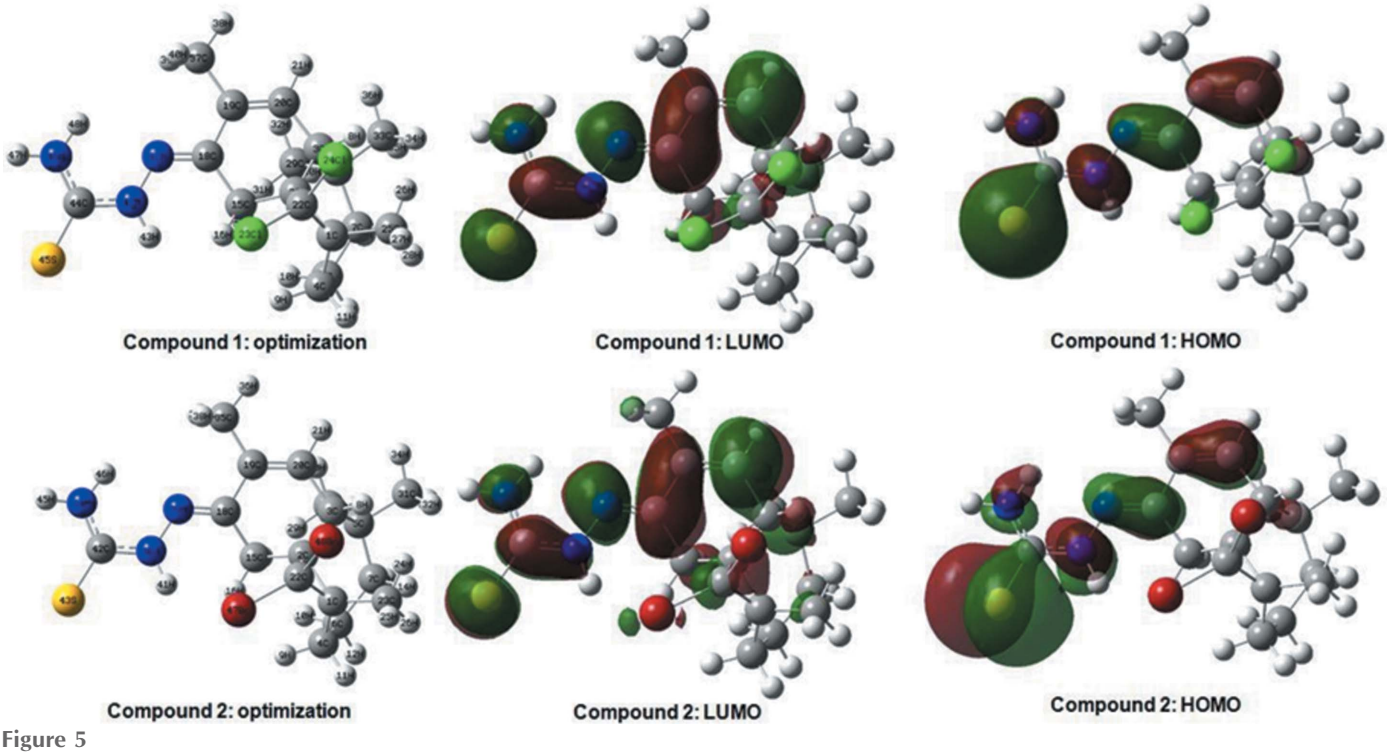

Figure 5
The optimized molecule and the HOMO and LUMO levels for thiosemicarbazone compounds **1** and **2** calculated with the B3LYP/6-31G(d) basis set.

and is a measure of the polarity of a polar covalent bond (BenHmamou *et al.*, 2015). Many authors report that the inhibition efficiency increases with an increase in the dipole-moment parameter which depends on the type and nature of the molecules considered, yet others suggested the opposite (Al-sabagh *et al.*, 2013). In general, it can be stated that the adsorption mode of the molecules depends holistically upon the involved polar functional groups interacting with a stainless steel surface, as well as the surface charge and the solution-dissolved ions. In fact, there is a lack of agreement in the literature on the correlation between dipole moment and the inhibition efficiency (Al-sabagh *et al.*, 2013). It is clearly seen

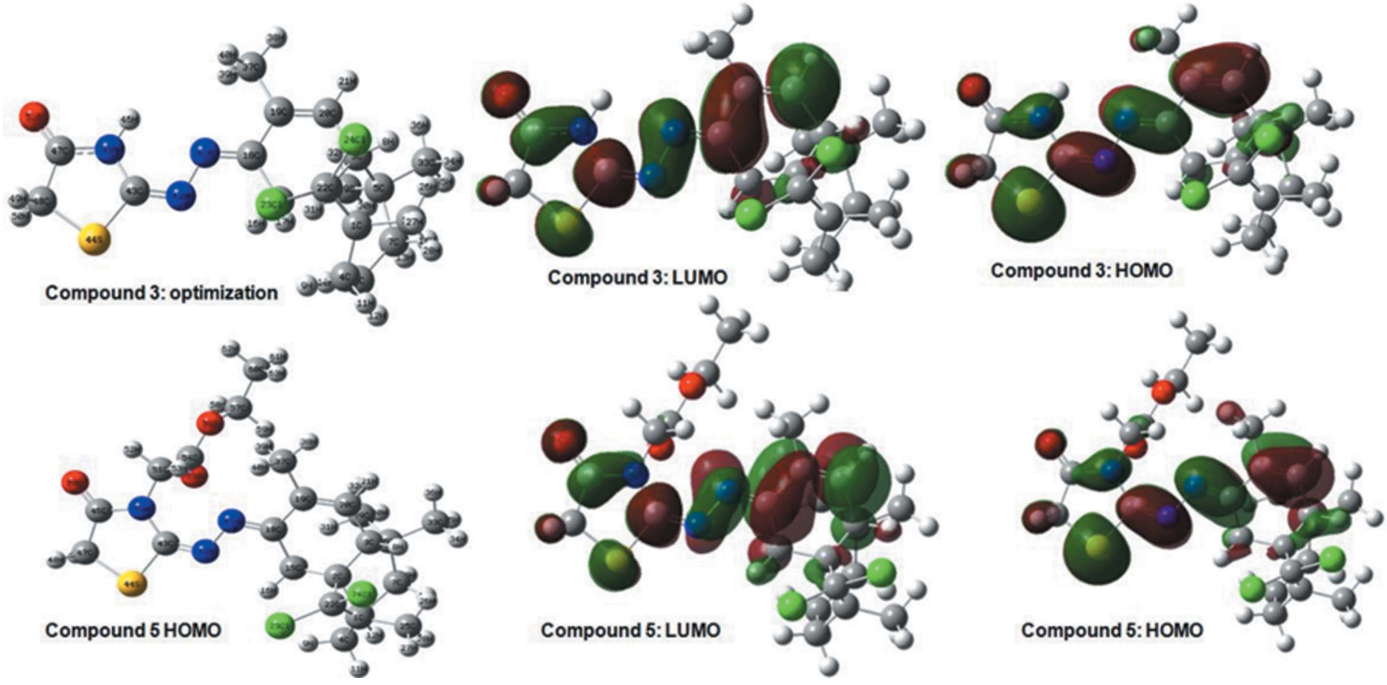

Figure 6
The optimized molecule and the HOMO and LUMO levels for thiazolidin-4-one compounds **3** and **5** calculated with the B3LYP/6-31G(d) basis set.

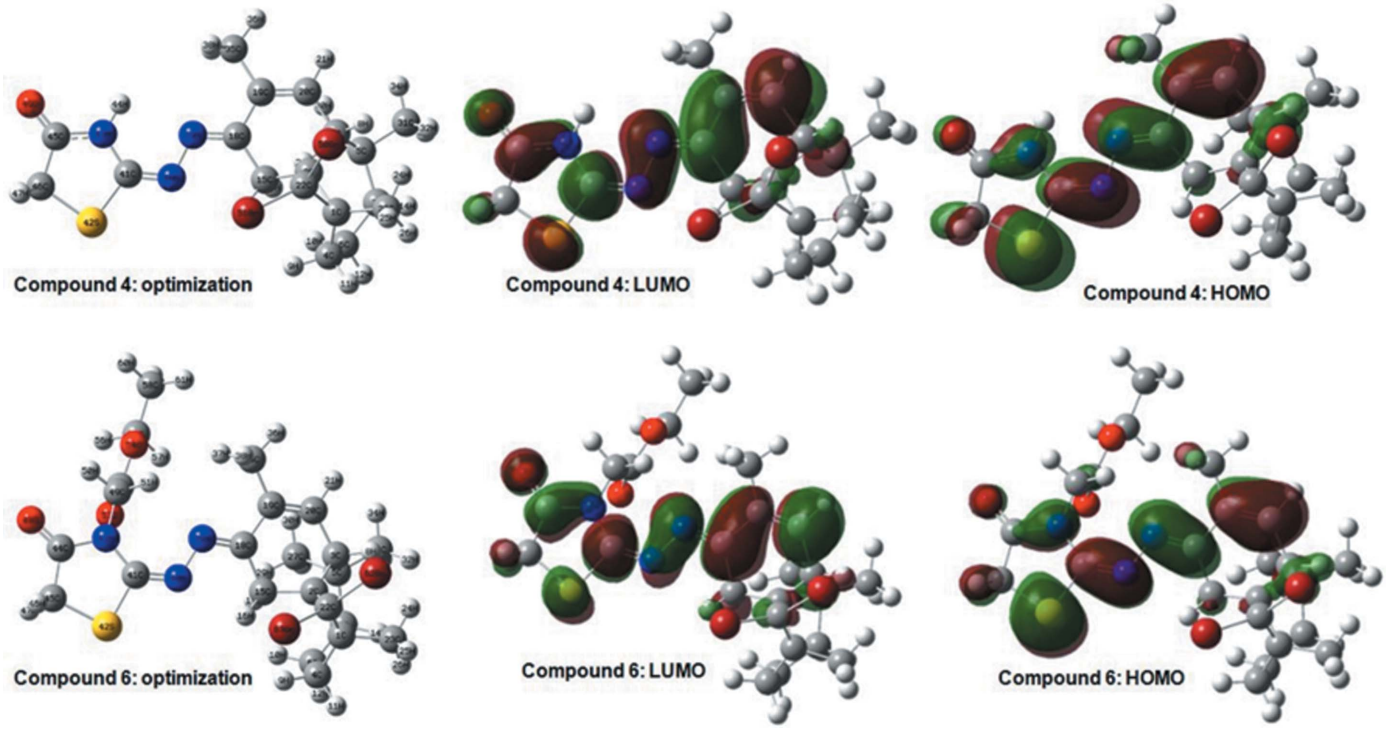

Figure 7
The optimized molecule and the HOMO and LUMO levels for thiazolidin-4-one compounds **4** and **6** calculated with the B3LYP/6-31G(d) basis set.

that the dipole moment of the investigated molecules follows the order **1** > **2** > **5** > **3** > **6** > **4** and the thiosemicarbazone compounds have higher values of the dipole moment with respect to the thiazolidin-4-one derivatives. The fractions of electrons transferred from inhibitor to metal surface were also determined (Table 7). According to Lukovits *et al.* (2001), if $\Delta N < 3.6$, the inhibition efficiency of a molecule increases with the increasing electron-donating ability at the metal surface. In the present case, the value of ΔN for all the tested derivatives is much higher than 3.6, which means that the increase in inhibition efficiency is not only due to the electron-donating ability of the inhibitor. From Table 7, we see that the values of the hardness for all molecules are positive ($\eta > 0$) and $\Delta E_T < 0$. This indicates that both donation and back-donation processes are responsible for the observed inhibition efficiency for all molecules (Klapper *et al.* 2013). Figs. 5, 6 and 7 show the HOMO, LUMO and optimized structures of the different studied molecules. It is clearly seen that both the HOMO and LUMO are predominantly made up of S and N atoms, as well as the C atoms implied in the conjugated system. The obtained theoretical results are in agreement with the experimental findings as the thiosemicarbazones have shown a good inhibition efficiency compared to the thiazolidin-4-one molecules.

4. Conclusion

In summary, we have prepared a new thiosemicarbazone and four new thiazolidin-4-ones using sesquiterpene hydrocarbon extracted from *Cedrus atlantica*. The substituted thiazolidin-4-ones were obtained by reacting the corresponding thiosemicarbazones with an excess of ethyl 2-bromoacetate. However, with an equivalent of ethyl 2-bromoacetate, we obtained the corresponding nonsubstituted thiazolidin-4-one. The compounds were characterized spectroscopically and compound **5** was also characterized by single-crystal X-ray diffraction. The results of the potentiodynamic polarization measurements indicated that all tested molecules act as mixed-type inhibitors. Thiosemicarbazone **2** showed a maximum inhibition efficiency of 92% at 10^{-3} *M*. The analysis of the different compounds has revealed that the thiosemicarbazone compounds could be more efficient than the thiazolidin-4-one derivatives. Quantum chemical calculations support the experimental findings. Based on the molecular properties of the different molecules, both donation and back donation are responsible for the inhibition efficiency. Cyclic voltammetry studies demonstrate that the thiosemicarbazone molecules have the lowest energy band gap, which substantiates the theoretical data.

Acknowledgements

The X-ray diffractometers are funded by Region NPDC, FEDER, CNRS and MESR.

References

Al-sabagh, A. M., Nasser, N. M., Migahed, M. A., Eissa, A. M. F. & Mahmoud, T. (2013). *Egypt. J. Pet.* **22**, 101–116.
Aries, R. (1974). Fr. Patent 2 186 245; *Chem. Abstr.* **81**, 140869.
Aries, R. (1975). Fr. Patent 2 190 431.
Aries, R. (1976). *Chem. Abstr.* **84**, 35329
Auhmani, A., Kossareva, E., Eljamili, H., Réglier, M., Pierrot, M. & Benharref, A. (2002). *Synth. Commun.* **32**, 699–707.

Auhmani, A., Kossareva, E., Lassaba, E., Réglier, M., Pierrot, M. & Benharref, A. (1999). *Acta Cryst.* C**55**, IUC9900055.

Becke, A. D. (1988). *Phys. Rev. A*, **38**, 3098–3100.

Benharref, A., Oukhrib, A., Ait Elhad, M., Daran, J. C. & Berraho, M. (2016). *IUCrData*, **1**, x160554.

BenHmamou, D., Salghi, R., Zarrouk, A., Zarrok, H., Touzani, R., Hammouti, B. & El Assyry, A. (2015). *J. Environ. Chem. Eng.* **3**, 2031–2041.

Bentiss, F., Lebrini, M., Lagrenée, M., Traisnel, M., Elfarouk, A. & Vezin, H. (2007). *Electrochim. Acta*, **52**, 6865–6872.

Blajiev, O. & Hubin, A. (2004). *Electrochim. Acta*, **49**, 2761–2770.

Bondock, S., Khalifa, W. & Fadda, A. A. (2006). *Synth. Commun*. **36**, 1601–1612.

Bondock, S., Khalifa, W. & Fadda, A. A. (2007). *Eur. J. Med. Chem*. **42**, 948–954.

Brandenburg, K. & Putz, H. (2012). *DIAMOND*. Crystal Impact GbR, Bonn, Germany.

Bruker (2012). *APEX2*, *SAINT* and *SADABS*. Bruker AXS Inc., Madison, Wisconsin, USA.

Chaudhary, M., Parmar, S. S., Chaudhary, S. K., Chaturvedi, A. K. & Rama Sastry, B. V. (1976). *J. Pharm. Sci*. **65**, 443–446.

Chaudhary, R. S., Tyagi, D. K., Rani, M. & Kumar, A. (2007). *J. Sci. Ind. Res*. **66**, 47–51.

Chaudhary, S. K., Verma, M., Chaturvedi, A. K. & Parmar, S. S. (1975). *J. Pharm. Sci*. **64**, 614–617.

Cremer, D. & Pople, J. A. (1975). *J. Am. Chem. Soc*. **97**, 1354–1358.

Cunico, W., Gomes, C. R. B., Ferreira, M. D. L., Capri, L. R., Soares, M. & Wardell, S. M. S. V. (2007). *Tetrahedron Lett*. **48**, 6217–6220.

Dandia, A., Singh, R., Khaturia, S., Me-rienne, C., Morgantc, G. & Loupyd, A. (2006). *Bioorg. Med. Chem*. **14**, 2409–2417.

Danila, G. & Radu, C. (1978). *Rev. Med. Chir*. **82**, 127–130.

Danila, G. & Radu, C. (1979). *Chem. Abstr*. **90**, 33767.

Das, J., Siram, R. B. K., Cahen, D., Rybtchinski, B. & Hodes, G. (2015). *J. Mater. Chem. A*, **3**, 20305–20312.

Desai, K. R. & Mistry, K. (2006). *Indian J. Chem. Sect. B*, **45**, 1762–1766.

Farrugia, L. J. (2012). *J. Appl. Cryst.* **45**, 849–854.

Fraga-Dubreuil, J. & Bazureau, J. P. (2003). *Tetrahedron*, **59**, 6121–6130.

Frisch M. J., *et al.* (2009). *GAUSSIAN09*. Revision A.01. Gaussian Inc., Wallingford, CT, USA. http://www.gaussian.com.

Gautam, D. & Chaudhary, R. P. (2015). *J. Mol. Struct.* **1080**, 137–144.

Gautam, D., Gautam, P. & Chaudhary, R. P. (2013). *Heterocycl. Commun*. **19**, 43–47.

Gece, G. (2008). *Corros. Sci.* **50**, 2981–2992.

Giraudon, R. (1972). Fr. Patent 2 108 834.

Giraudon, R. (1973). *Chem. Abstr*. **79**, 32040.

Gudduduru, V., Hurth, E., Dalton, J. T. & Miller, D. D. (2004). *Bioorg. Med. Chem. Lett*. **14**, 5289–5293.

Gupta, R. & Chaudhary, R. P. (2013). *Phosphorus Sulfur Silicon*, **188**, 1296–1304.

Hassan, A. A., Mohamed, S. K., Mohamed, N. K., El-Shaieb, K. M. A., Abdel-Aziz, A. T., Mague, J. T. & Akkurt, M. (2017). *J. Heterocycl. Chem.* **54**, 2043–2053.

Holmes, C., Chinn, J. P., Look, G. C., Gordon, E. M. & Gallop, M. A. (1995). *J. Org. Chem*. **60**, 7328–7333.

Idouhli, R., N'Ait Ousidi, A., Koumya, Y., Abouelfida, A., Benyaich, A., Auhmani, A. & Ait Itto, M. Y. (2018*a*). *Int. J. Corros.* pp. 1–15.

Idouhli, R., Oukhrib, A., Koumya, Y., Abouelfida, A., Benyaich, A. & Benharref, A. (2018*b*). *Corros Rev*. **36**, 373–384.

Klapper, H. S., Goellner, J., Burkert, A. & Hegn, A. (2013). *Corros. Sci.* **75**, 239–247.

Lebrini, M., Lagrene, M., Traisnel, M., Gengembre, L., Vezin, H. & Bentiss, F. (2007). *Appl. Surf. Sci*. **253**, 9267–9276.

Lee, C., Yang, W. & Parr, R. G. (1988). *Phys. Rev. B*, **37**, 785–789.

Li, L., Zhang, X., Lei, J., He, J., Zhang, S. & Pan, F. (2012). *Corros. Sci*. **63**, 82–90.

Li, Z., Dong, Q., Li, Y., Xu, B., Deng, M., Pei, J., Zhang, J., Chen, F., Wen, S., Gao, Y. & Tian, W. (2011). *J. Mater. Chem.* **21**, 2159–2168.

Lukovits, I., Kálmán, E. & Zucchi, F. (2001). *Corrosion*, **57**, 3–8.

Maclean, D., Holden, F., Davis, A. M., Scheuerman, R. A., Yanofsky, S., Holmes, C. P., Fitch, W. L., Tsutsui, K., Barrett, R. W. & Gallop, M. A. (2004). *J. Comb. Chem*. **6**, 196–206.

Mague, J. T., Akkurt, M., Mohamed, S. K., Hassan, A. A. & Albayati, M. R. (2014). *Acta Cryst.* E**70**, o436–o437.

Misra, N. C. & Patnayak, K. K. (1971). *Indian J. Appl. Chem*. **34**, 148–155.

Mourya, P., Banerjee, S., Rastogi, R. B. & Singh, M. M. (2013). *ACS Ind. Eng. Chem. Res*. **52**, 12733–12747.

Nagar, S., Singh, H. H., Sinha, J. N. & Parmar, S. S. (1973). *J. Med. Chem.* **16**, 178–180.

N'ait Ousidi, A., Ait Itto, M. Y., Auhmani, A., Riahi, A., Auhmani, A. & Daran, J.-C. (2017). *Acta Cryst.* E**73**, 296–299.

Ottana, R., Carotti, S., Maccari, R., Landini, I., Chiricosta, G., Caciagli, B., Vigorita, M. G. & Mini, E. (2005*a*). *Bioorg. Med. Chem. Lett*. **15**, 3930–3933.

Ottana, R., Maccari, R., Barreca, M. L., Bruno, G., Rotondo, A., Rossi, A., Chiricosta, G., Di Paola, R., Sautebin, L., Cuzzocread, S. & Vigorita, M. G. (2005*b*). *Bioorg. Med. Chem*. **13**, 4243–4252.

Ottana, R., Mazzon, E., Dugo, L., Monforte, F., Maccari, R., Sautebin, L., De Luca, G., Vigorita, M. G., Alcaro, S., Ortuso, F., Caputi, A. P. & Cuzzocrea, S. (2002). *Eur. J. Pharmacol*. **448**, 71–80.

Ourhriss, N., Giorgi, M., Mazoir, N. & Benharref, A. (2005). *Acta Cryst.* C**61**, o699–o701.

Parmar, S. S., Dwivedi, C., Chaudhari, A. & Gupta, T. K. (1972). *J. Med. Chem*. **15**, 99–101.

Parsons, S., Flack, H. D. & Wagner, T. (2013). *Acta Cryst.* B**69**, 249–259.

Patel, N. S., Jauhariand, S., Mehta, G. N., Al-Deyab, S. S., Warad, I. & Hammouti, B. (2013). *Int. J. Electrochem. Sci.* **8**, 2635–2655.

Pyo, H., Choy, H., Amorino, G. P., Kim, J. S., Cao, Q., Hercules, S. K. & DuBois, R. N. (2001). *Clin. Cancer Res.* **7**, 2998–3005.

Ramachandran, R., Rani, M. & Kabilan, S. (2009). *Acta Cryst.* E**65**, o584.

Rawal, R. K., Prabhakar, Y. S., Katti, S. B. & De Clercq, E. (2005). *Bioorg. Med. Chem*. **13**, 6771–6776.

Sheldrick, G. M. (2008). *Acta Cryst.* A**64**, 112–122.

Sheldrick, G. M. (2015). *Acta Cryst.* C**71**, 3–8.

Shyam, R. & Tiwari, I. C. (1977). *Bull. Chem. Soc. Jpn*, **50**, 514–516.

Singh, A. & Chaudhary, R. S. (1996). *Br. Corros. J.* **31**, 300–304.

Singh, S. P., Parmar, S. S., Raman, K. & Stenberg, V. I. (1981). *Chem. Rev.* **81**, 175–203.

Srivastava, T., Gaikwad, A. K., Haq, W., Sinha, S. & Katti, S. B. (2005). *Arkivoc*, **ii**, 120–130.

Suzuki, Y., Akima, M. & Tamura, K. (1999). *Gen. Pharmacol*. **32**, 57–63.

Vicini, P., Geronikaki, A., Anastasia, K., Incertia, M. & Zania, F. (2006). *Bioorg. Med. Chem*. **14**, 3859–3864.

Vigorita, M. G., Ottana, R., Monforte, F., Maccari, R., Monforte, M. T., Trovato, A., Taviano, M. F., Miceli, N., De Luca, G., Alcaro, S. & Ortuso, F. (2003). *Bioorg. Med. Chem*. **11**, 999–1006.

Zubenky, V. G., Ladnaya, L. Y., Turkevich, N. M. & Tatchinkapustyak, S. M. (1974). *Farm. Zh*. **29**, 78.

Zubenky, V. G., Ladnaya, L. Y., Turkevich, N. M. & Tatchinkapustyak, S. M. (1975). *Chem. Abstr*. **82**, 667.

supporting information

Hemisynthesis, crystal structure and inhibitory effect of sesquiterpenic thiosemicarbazones and thiazolidin-4-ones on the corrosion behaviour of stainless steel in 1 *M* H_2SO_4 solution

Abdoullah Bimoussa, Yassine Koumya, Abdesselam Abouelfida, Moulay Youssef Ait Itto, Abdelaziz Benyaich, Olivier Mentre, El Mostafa Ketatni, Aziz Auhmani and Abdelwahed Auhmani

Computing details

Data collection: DUO in *APEX2* (Bruker, 2012); cell refinement: *SAINT* (Bruker, 2012); data reduction: *SAINT* (Bruker, 2012); program(s) used to solve structure: *SHELXS2014* (Sheldrick, 2008); program(s) used to refine structure: *SHELXL2014* (Sheldrick, 2015); molecular graphics: *ORTEP-3 for Windows* (Farrugia, 2012) and *DIAMOND* (Brandenburg & Putz, 2012); software used to prepare material for publication: *SHELXL2014* (Sheldrick, 2015).

Ethyl 2-{(*Z*)-2-{(*Z*)-[(1a*R*,5a*R*,9a*S*)-1,1-dichloro-1a,5,5,7-tetramethyl-1a,2,3,4,5,5a,8,9-octahydro-1*H*-benzo[*a*]cyclopropa[*b*][7]annulen-8-ylidene]hydrazono}-4-oxothiazolidin-3-yl)acetate

Crystal data

$C_{23}H_{31}Cl_2N_3O_3S$
M_r = 500.47
Orthorhombic, $P2_12_12_1$
a = 10.2769 (7) Å
b = 12.2445 (7) Å
c = 20.0804 (13) Å
V = 2526.8 (3) Å^3
Z = 4
$F(000)$ = 1056
D_x = 1.316 Mg m^{-3}
Mo $K\alpha$ radiation, λ = 0.71073 Å
Cell parameters from 5789 reflections
θ = 2.0–27.5°
μ = 0.37 mm^{-1}
T = 299 K
Block, colourless
0.34 × 0.21 × 0.11 mm

Data collection

Bruker DUO APEXII CCD diffractometer
φ and ω scans
Absorption correction: multi-scan (SADABS; Bruker, 2012)
T_{min} = 0.710, T_{max} = 0.746
58280 measured reflections
5789 independent reflections
4306 reflections with $I > 2\sigma(I)$
R_{int} = 0.056
θ_{max} = 27.5°, θ_{min} = 2.0°
h = −13→13
k = −15→15
l = −25→25

Refinement

Refinement on F^2
Least-squares matrix: full
$R[F^2 > 2\sigma(F^2)]$ = 0.038
$wR(F^2)$ = 0.089
S = 1.03
5789 reflections
294 parameters
0 restraints

Hydrogen site location: inferred from neighbouring sites
H-atom parameters constrained
$w = 1/[\sigma^2(F_o^2) + (0.0393P)^2 + 0.3269P]$ where $P = (F_o^2 + 2F_c^2)/3$
$(\Delta/\sigma)_{max} < 0.001$
$\Delta\rho_{max} = 0.26$ e Å^{-3}
$\Delta\rho_{min} = -0.19$ e Å^{-3}
Absolute structure: Flack *x* determined using 1538 quotients [(I+)-(I-)]/[(I+)+(I-)] (Parsons *et al.*, 2013)
Absolute structure parameter: −0.04 (2)

Special details

Geometry. All esds (except the esd in the dihedral angle between two l.s. planes) are estimated using the full covariance matrix. The cell esds are taken into account individually in the estimation of esds in distances, angles and torsion angles; correlations between esds in cell parameters are only used when they are defined by crystal symmetry. An approximate (isotropic) treatment of cell esds is used for estimating esds involving l.s. planes.

Fractional atomic coordinates and isotropic or equivalent isotropic displacement parameters (Å²)

	x	*y*	*z*	U_{iso}*/U_{eq}
Cl1	0.91689 (9)	0.40874 (6)	0.28176 (4)	0.0521 (2)
Cl2	0.92163 (8)	0.64247 (6)	0.28263 (4)	0.0456 (2)
S1′	0.41368 (9)	0.18868 (7)	0.16736 (5)	0.0572 (3)
O1	0.5447 (3)	−0.10510 (19)	0.14607 (15)	0.0719 (8)
O2	0.7293 (3)	0.0766 (2)	0.02640 (14)	0.0716 (8)
O3	0.9255 (3)	0.0866 (3)	0.07238 (13)	0.0816 (9)
N1	0.6044 (2)	0.3561 (2)	0.15782 (13)	0.0447 (6)
N2	0.6657 (3)	0.2530 (2)	0.15405 (14)	0.0441 (7)
N3′	0.6216 (2)	0.06903 (19)	0.15379 (14)	0.0447 (7)
C1	0.9428 (3)	0.5258 (2)	0.23193 (14)	0.0334 (6)
C1A	1.0446 (3)	0.5220 (2)	0.17788 (15)	0.0341 (7)
C2	1.1211 (3)	0.6249 (2)	0.16433 (16)	0.0418 (7)
H2A	1.2050	0.6198	0.1863	0.050*
H2B	1.0751	0.6868	0.1831	0.050*
C3	1.1421 (3)	0.6439 (3)	0.08995 (18)	0.0538 (9)
H3A	1.2185	0.6032	0.0761	0.065*
H3B	1.1605	0.7208	0.0830	0.065*
C4	1.0282 (3)	0.6115 (3)	0.04491 (17)	0.0509 (9)
H4A	1.0515	0.6310	−0.0004	0.061*
H4B	1.0207	0.5326	0.0464	0.061*
C5	0.8934 (3)	0.6590 (2)	0.05887 (15)	0.0425 (8)
C5A	0.8460 (3)	0.6323 (2)	0.13161 (14)	0.0338 (7)
H5A	0.8799	0.6908	0.1600	0.041*
C6	0.7006 (3)	0.6342 (3)	0.13993 (15)	0.0406 (7)
H6	0.6597	0.7019	0.1379	0.049*
C7	0.6253 (3)	0.5472 (2)	0.14991 (15)	0.0387 (7)
C8	0.6826 (3)	0.4371 (2)	0.14911 (15)	0.0357 (7)
C9	0.8265 (3)	0.4258 (2)	0.13597 (16)	0.0361 (7)
H9A	0.8412	0.4166	0.0886	0.043*
H9B	0.8594	0.3614	0.1585	0.043*
C9A	0.8990 (3)	0.5258 (2)	0.16040 (13)	0.0300 (6)
C10	1.1226 (3)	0.4187 (2)	0.16751 (19)	0.0466 (8)
H10A	1.0659	0.3566	0.1703	0.070*

H10B	1.1885	0.4134	0.2013	0.070*
H10C	1.1630	0.4206	0.1244	0.070*
C11	0.8944 (4)	0.7841 (3)	0.05106 (19)	0.0587 (10)
H11A	0.9255	0.8029	0.0074	0.088*
H11B	0.9507	0.8156	0.0840	0.088*
H11C	0.8078	0.8119	0.0568	0.088*
C12	0.8010 (4)	0.6128 (3)	0.00546 (17)	0.0591 (10)
H12A	0.8294	0.6361	−0.0378	0.089*
H12B	0.7143	0.6389	0.0134	0.089*
H12C	0.8017	0.5344	0.0075	0.089*
C13	0.4803 (3)	0.5579 (3)	0.1594 (2)	0.0581 (10)
H13A	0.4360	0.5206	0.1240	0.087*
H13B	0.4566	0.6338	0.1589	0.087*
H13C	0.4560	0.5263	0.2013	0.087*
C2′	0.5817 (3)	0.1767 (2)	0.15774 (15)	0.0414 (7)
C4′	0.5249 (3)	−0.0091 (3)	0.15382 (17)	0.0501 (9)
C5′	0.3940 (3)	0.0420 (3)	0.1651 (2)	0.0565 (9)
H5′A	0.3576	0.0164	0.2068	0.068*
H5′B	0.3351	0.0218	0.1294	0.068*
C6′	0.7568 (3)	0.0426 (3)	0.14311 (17)	0.0479 (8)
H6′A	0.7701	−0.0348	0.1508	0.057*
H6′B	0.8099	0.0826	0.1748	0.057*
C7′	0.7990 (4)	0.0707 (3)	0.07342 (19)	0.0493 (9)
C8′	0.9852 (5)	0.1165 (6)	0.0093 (2)	0.1041 (19)
H8′A	1.0096	0.0512	−0.0151	0.125*
H8′B	0.9239	0.1576	−0.0176	0.125*
C9′	1.0974 (7)	0.1811 (5)	0.0221 (3)	0.133 (3)
H9′A	1.1409	0.1969	−0.0191	0.199*
H9′B	1.1553	0.1417	0.0510	0.199*
H9′C	1.0718	0.2481	0.0431	0.199*

Atomic displacement parameters (Å²)

	U^{11}	U^{22}	U^{33}	U^{12}	U^{13}	U^{23}
Cl1	0.0539 (5)	0.0422 (4)	0.0601 (5)	0.0043 (4)	0.0065 (5)	0.0198 (4)
Cl2	0.0503 (5)	0.0425 (4)	0.0441 (4)	0.0020 (4)	−0.0012 (4)	−0.0076 (3)
S1′	0.0366 (5)	0.0501 (5)	0.0849 (7)	−0.0068 (4)	0.0104 (5)	−0.0062 (4)
O1	0.076 (2)	0.0378 (13)	0.102 (2)	−0.0106 (12)	0.0121 (16)	−0.0047 (13)
O2	0.0620 (19)	0.097 (2)	0.0559 (17)	−0.0111 (16)	−0.0092 (16)	−0.0069 (14)
O3	0.0451 (18)	0.150 (3)	0.0499 (16)	−0.0113 (19)	0.0077 (14)	0.0047 (16)
N1	0.0343 (15)	0.0404 (13)	0.0595 (17)	−0.0021 (13)	0.0024 (13)	−0.0069 (12)
N2	0.0354 (15)	0.0366 (14)	0.0602 (18)	−0.0060 (12)	0.0039 (14)	−0.0043 (12)
N3′	0.0388 (17)	0.0356 (13)	0.0597 (18)	−0.0024 (11)	0.0036 (14)	−0.0034 (12)
C1	0.0333 (17)	0.0264 (13)	0.0404 (16)	0.0001 (13)	−0.0001 (13)	0.0027 (12)
C1A	0.0274 (16)	0.0292 (13)	0.0456 (17)	0.0018 (12)	0.0017 (13)	0.0024 (13)
C2	0.0284 (17)	0.0387 (16)	0.058 (2)	−0.0035 (13)	0.0029 (15)	0.0018 (14)
C3	0.041 (2)	0.056 (2)	0.065 (2)	−0.0024 (17)	0.0117 (18)	0.0132 (18)
C4	0.052 (2)	0.053 (2)	0.047 (2)	0.0064 (17)	0.0104 (17)	0.0089 (16)

C5	0.049 (2)	0.0374 (16)	0.0415 (18)	0.0039 (15)	−0.0017 (16)	0.0042 (12)
C5A	0.0336 (17)	0.0287 (14)	0.0391 (16)	0.0035 (13)	−0.0022 (13)	0.0010 (12)
C6	0.0351 (18)	0.0371 (16)	0.0496 (19)	0.0112 (14)	−0.0046 (15)	0.0006 (14)
C7	0.0298 (17)	0.0434 (17)	0.0429 (18)	0.0051 (13)	−0.0020 (14)	−0.0071 (13)
C8	0.0289 (17)	0.0377 (16)	0.0406 (18)	−0.0004 (13)	−0.0006 (14)	−0.0046 (13)
C9	0.0288 (17)	0.0292 (14)	0.0501 (19)	0.0032 (12)	0.0006 (14)	−0.0034 (13)
C9A	0.0245 (15)	0.0264 (12)	0.0392 (15)	0.0025 (12)	0.0007 (13)	−0.0014 (12)
C10	0.0324 (18)	0.0387 (16)	0.069 (2)	0.0074 (14)	0.0046 (17)	0.0030 (15)
C11	0.073 (3)	0.0444 (19)	0.059 (2)	0.003 (2)	−0.004 (2)	0.0173 (15)
C12	0.069 (3)	0.061 (2)	0.048 (2)	0.007 (2)	−0.0091 (19)	0.0008 (17)
C13	0.033 (2)	0.066 (2)	0.075 (3)	0.0113 (17)	−0.0009 (19)	−0.011 (2)
C2′	0.0361 (17)	0.0424 (16)	0.0456 (18)	−0.0061 (15)	0.0042 (16)	−0.0044 (13)
C4′	0.051 (2)	0.046 (2)	0.054 (2)	−0.0124 (16)	0.0059 (17)	0.0001 (16)
C5′	0.044 (2)	0.054 (2)	0.071 (2)	−0.0187 (17)	0.0089 (19)	−0.0073 (17)
C6′	0.040 (2)	0.0479 (19)	0.056 (2)	0.0009 (16)	0.0027 (16)	−0.0011 (16)
C7′	0.043 (2)	0.051 (2)	0.053 (2)	−0.0010 (17)	0.0023 (19)	−0.0078 (16)
C8′	0.069 (3)	0.194 (6)	0.049 (3)	−0.023 (4)	0.021 (2)	−0.005 (3)
C9′	0.171 (7)	0.148 (5)	0.079 (4)	−0.076 (5)	0.042 (4)	−0.027 (3)

Geometric parameters (Å, º)

Cl1—C1	1.768 (3)	C5A—H5A	0.9800
Cl2—C1	1.768 (3)	C6—C7	1.332 (4)
S1′—C2′	1.744 (3)	C6—H6	0.9300
S1′—C5′	1.808 (3)	C7—C8	1.472 (4)
O1—C4′	1.203 (4)	C7—C13	1.508 (5)
O2—C7′	1.188 (4)	C8—C9	1.509 (4)
O3—C7′	1.315 (5)	C9—C9A	1.515 (4)
O3—C8′	1.455 (5)	C9—H9A	0.9700
N1—C8	1.288 (4)	C9—H9B	0.9700
N1—N2	1.413 (3)	C10—H10A	0.9600
N2—C2′	1.274 (4)	C10—H10B	0.9600
N3′—C4′	1.380 (4)	C10—H10C	0.9600
N3′—C2′	1.383 (4)	C11—H11A	0.9600
N3′—C6′	1.442 (4)	C11—H11B	0.9600
C1—C9A	1.505 (4)	C11—H11C	0.9600
C1—C1A	1.508 (4)	C12—H12A	0.9600
C1A—C2	1.509 (4)	C12—H12B	0.9600
C1A—C10	1.512 (4)	C12—H12C	0.9600
C1A—C9A	1.538 (4)	C13—H13A	0.9600
C2—C3	1.527 (5)	C13—H13B	0.9600
C2—H2A	0.9700	C13—H13C	0.9600
C2—H2B	0.9700	C4′—C5′	1.501 (5)
C3—C4	1.532 (5)	C5′—H5′A	0.9700
C3—H3A	0.9700	C5′—H5′B	0.9700
C3—H3B	0.9700	C6′—C7′	1.505 (5)
C4—C5	1.529 (5)	C6′—H6′A	0.9700
C4—H4A	0.9700	C6′—H6′B	0.9700

C4—H4B	0.9700	C8′—C9′	1.421 (7)
C5—C11	1.539 (4)	C8′—H8′A	0.9700
C5—C12	1.540 (5)	C8′—H8′B	0.9700
C5—C5A	1.574 (4)	C9′—H9′A	0.9600
C5A—C6	1.504 (4)	C9′—H9′B	0.9600
C5A—C9A	1.527 (4)	C9′—H9′C	0.9600

C2′—S1′—C5′	91.40 (15)	C1—C9A—C9	117.1 (2)
C7′—O3—C8′	117.9 (3)	C1—C9A—C5A	117.9 (2)
C8—N1—N2	113.7 (2)	C9—C9A—C5A	113.1 (2)
C2′—N2—N1	110.5 (3)	C1—C9A—C1A	59.40 (19)
C4′—N3′—C2′	116.6 (3)	C9—C9A—C1A	121.9 (2)
C4′—N3′—C6′	122.6 (3)	C5A—C9A—C1A	117.3 (2)
C2′—N3′—C6′	120.5 (3)	C1A—C10—H10A	109.5
C9A—C1—C1A	61.37 (18)	C1A—C10—H10B	109.5
C9A—C1—Cl1	119.7 (2)	H10A—C10—H10B	109.5
C1A—C1—Cl1	119.2 (2)	C1A—C10—H10C	109.5
C9A—C1—Cl2	120.84 (19)	H10A—C10—H10C	109.5
C1A—C1—Cl2	121.6 (2)	H10B—C10—H10C	109.5
Cl1—C1—Cl2	108.09 (15)	C5—C11—H11A	109.5
C1—C1A—C2	117.8 (2)	C5—C11—H11B	109.5
C1—C1A—C10	119.5 (2)	H11A—C11—H11B	109.5
C2—C1A—C10	113.4 (2)	C5—C11—H11C	109.5
C1—C1A—C9A	59.22 (18)	H11A—C11—H11C	109.5
C2—C1A—C9A	116.2 (2)	H11B—C11—H11C	109.5
C10—C1A—C9A	120.6 (2)	C5—C12—H12A	109.5
C1A—C2—C3	112.2 (3)	C5—C12—H12B	109.5
C1A—C2—H2A	109.2	H12A—C12—H12B	109.5
C3—C2—H2A	109.2	C5—C12—H12C	109.5
C1A—C2—H2B	109.2	H12A—C12—H12C	109.5
C3—C2—H2B	109.2	H12B—C12—H12C	109.5
H2A—C2—H2B	107.9	C7—C13—H13A	109.5
C2—C3—C4	115.5 (3)	C7—C13—H13B	109.5
C2—C3—H3A	108.4	H13A—C13—H13B	109.5
C4—C3—H3A	108.4	C7—C13—H13C	109.5
C2—C3—H3B	108.4	H13A—C13—H13C	109.5
C4—C3—H3B	108.4	H13B—C13—H13C	109.5
H3A—C3—H3B	107.5	N2—C2′—N3′	119.6 (3)
C5—C4—C3	119.1 (3)	N2—C2′—S1′	128.0 (2)
C5—C4—H4A	107.6	N3′—C2′—S1′	112.3 (2)
C3—C4—H4A	107.6	O1—C4′—N3′	123.8 (3)
C5—C4—H4B	107.6	O1—C4′—C5′	125.3 (3)
C3—C4—H4B	107.6	N3′—C4′—C5′	110.9 (3)
H4A—C4—H4B	107.0	C4′—C5′—S1′	108.5 (2)
C4—C5—C11	110.7 (3)	C4′—C5′—H5′A	110.0
C4—C5—C12	106.9 (3)	S1′—C5′—H5′A	110.0
C11—C5—C12	107.4 (3)	C4′—C5′—H5′B	110.0
C4—C5—C5A	111.8 (3)	S1′—C5′—H5′B	110.0

C11—C5—C5A	107.7 (3)	H5′A—C5′—H5′B	108.4
C12—C5—C5A	112.3 (3)	N3′—C6′—C7′	111.4 (3)
C6—C5A—C9A	109.0 (2)	N3′—C6′—H6′A	109.3
C6—C5A—C5	114.0 (2)	C7′—C6′—H6′A	109.3
C9A—C5A—C5	114.7 (2)	N3′—C6′—H6′B	109.3
C6—C5A—H5A	106.1	C7′—C6′—H6′B	109.3
C9A—C5A—H5A	106.1	H6′A—C6′—H6′B	108.0
C5—C5A—H5A	106.1	O2—C7′—O3	125.1 (4)
C7—C6—C5A	125.5 (3)	O2—C7′—C6′	125.4 (3)
C7—C6—H6	117.2	O3—C7′—C6′	109.5 (3)
C5A—C6—H6	117.2	C9′—C8′—O3	108.9 (4)
C6—C7—C8	119.9 (3)	C9′—C8′—H8′A	109.9
C6—C7—C13	121.6 (3)	O3—C8′—H8′A	109.9
C8—C7—C13	118.5 (3)	C9′—C8′—H8′B	109.9
N1—C8—C7	117.0 (3)	O3—C8′—H8′B	109.9
N1—C8—C9	124.4 (3)	H8′A—C8′—H8′B	108.3
C7—C8—C9	118.6 (3)	C8′—C9′—H9′A	109.5
C8—C9—C9A	110.5 (2)	C8′—C9′—H9′B	109.5
C8—C9—H9A	109.5	H9′A—C9′—H9′B	109.5
C9A—C9—H9A	109.5	C8′—C9′—H9′C	109.5
C8—C9—H9B	109.5	H9′A—C9′—H9′C	109.5
C9A—C9—H9B	109.5	H9′B—C9′—H9′C	109.5
H9A—C9—H9B	108.1		

Hydrogen-bond geometry (Å, º)

D—H···*A*	*D*—H	H···*A*	*D*···*A*	*D*—H···*A*
C10—H10*A*···Cl2^{i}	0.96	2.79	3.557 (3)	137
C2—H2*B*···Cl1^{ii}	0.97	2.81	3.661 (3)	147

Symmetry codes: (i) −*x*+2, *y*−1/2, −*z*+1/2; (ii) −*x*+2, *y*+1/2, −*z*+1/2.